Impacts of updated reaction kinetics on the global GEOS-Chem simulation of atmospheric chemistry

Kelvin H. Bates[1,2], Mathew J. Evans[3,4], Barron H. Henderson[5], and Daniel J. Jacob[1]

[1]School of Engineering and Applied Sciences, Harvard University, Cambridge, MA 02138, USA
[2]NOAA Chemical Sciences Laboratory, Earth System Research Laboratories, & Cooperative Institute for Research in Environmental Sciences, University of Colorado, Boulder, CO 80305, USA
[3]Wolfson Atmospheric Chemistry Laboratories, Department of Chemistry, University of York, York, UK
[4]National Centre for Atmospheric Science, University of York, York, UK
[5]U.S. Environmental Protection Agency, Research Triangle Park, NC 27711, USA

Correspondence: Kelvin Bates (kelvin.bates@noaa.gov)

Abstract.

We updated the chemical mechanism of the GEOS-Chem global 3-D model of atmospheric chemistry to include new recommendations from the JPL chemical kinetics Data Evaluation 19-5 and from IUPAC, and to balance carbon and nitrogen. We examined the impact of these updates on the GEOS-Chem version 14.0.1 simulation. Notable changes include: eleven updates to reactions of reactive nitrogen species, resulting in a 7% net increase in the stratospheric NO_x ($NO + NO_2$) burden; an updated $CO + OH$ rate formula leading to a 2.7% reduction in total tropospheric CO; adjustments to the rate coefficient and branching ratios of propane + OH, leading to reduced tropospheric propane (-17%) and increased acetone (+3.5%) burdens; a 41% increase in the tropospheric burden of peroxyacetic acid due to a decrease in the rate coefficient for its reaction with OH, further contributing to reductions in peroxyacetyl nitrate (PAN; -3.8%) and acetic acid (-3.4%); and a number of minor adjustments to halogen radical cycling. Changes to the global tropospheric burdens of other species include -0.7% for ozone, +0.3% for OH (-0.4% for methane lifetime against oxidation by tropospheric OH), +0.8% for formaldehyde, and -1.7% for NO_x. The updated mechanism reflects the current state of the science including complex chemical dependencies of key atmospheric species on temperature, pressure, and concentrations of other compounds. The improved conservation of carbon and nitrogen will facilitate future studies of their overall atmospheric budgets.

1 Introduction

Chemical reactions underpin the trace gas composition of the atmosphere, removing some pollutants and climate forcing species while forming others. Accurate representation of reaction rate coefficients and product distributions of these reactions is crucial for atmospheric chemistry models. The NASA Jet Propulsion Laboratory (JPL) regularly assembles a panel of experts to assess and compile new data for rate constants and other key reaction parameters relevant to atmospheric chemistry. This panel produces data evaluations entitled "Chemical Kinetics and Photochemical Data for Use in Atmospheric Studies". Recommendations are predominantly based on laboratory measurements, although they may also be informed by computational

studies or by analogy to similar reactions when required, and are not adjusted to fit ambient observations. Where assessed experimental studies disagree on reaction parameters, the panel attempts to reconcile and/or arbitrate differences and provide estimated uncertainty bounds. A parallel evaluation process is conducted by the International Union of Pure and Applied

25 Chemistry (IUPAC) with more emphasis on organic chemistry (Atkinson et al., 2006).

Here, we update the chemical mechanism in the GEOS-Chem global atmospheric chemistry model with recommendations from the latest JPL Data Evaluation (Burkholder et al., 2020) and recent IUPAC updates (Mellouki et al., 2021). The GEOS-Chem model is used by hundreds of research groups worldwide for global and regional studies of tropospheric and stratospheric chemistry (http://geos-chem.org), and is also used as a chemistry module in meteorological and climate models (Hu et al.,

30 2018; Lin et al., 2021; Fritz et al., 2022). We enforce carbon and nitrogen conservation in a further 63 reactions to facilitate budget analyses (Safieddine et al., 2017). We examine the effects of these different changes on the GEOS-Chem simulation as documentation for their inclusion in the standard version of the model.

2   GEOS-Chem chemical mechanism updates

The GEOS-Chem model includes a detailed mechanism for oxidant-aerosol chemistry in the troposphere and stratosphere.

35 Since its first iteration as a model of tropospheric oxidant chemistry (Bey et al., 2001), the standard GEOS-Chem chemical mechanism has used kinetics and products based on JPL recommendations (DeMore et al., 1997). The model was later expanded to include aerosol chemistry (Park et al., 2004) and stratospheric chemistry (Eastham et al., 2014), and reaction rates and products were updated based on subsequent JPL data evaluations (Sander et al., 2006, 2011; Burkholder et al., 2015). Photolysis frequencies are calculated with the Fast-JX code (Bian and Prather, 2002) as implemented in GEOS-Chem by Mao

40 et al. (2010) for the troposphere and Eastham et al. (2014) for the stratosphere. Subsequent additions to the mechanism, such as detailed halogen chemistry (initially from Sherwen et al. 2016 and Chen et al. 2017, subsequently updated by Wang et al. 2021) as well as schemes for the oxidation of isoprene (initially from Mao et al. 2013, updated by Marais et al. 2016 and Bates and Jacob 2019), monoterpenes (Fisher et al., 2016), and aromatics (Bates et al., 2021), include reactions not assessed in the JPL data evaluations; kinetics and products of these reactions use recommendations from IUPAC (Atkinson et al., 2006) or

45 other sources detailed in the publications describing each update. More information on the GEOS-Chem mechanism can be found in the model documentation at http://www.geos-chem.org.

Here we focus on gas-phase thermal chemistry updates as given by JPL and IUPAC. Rate coefficients from the latest JPL recommendations are prioritized over those from IUPAC, the latter of which are only implemented for reactions of oxygenated organics not included in the JPL data evaluation. We do not include photolysis updates, as these are not significantly changed

50 in the latest JPL publication for reactions included in GEOS-Chem, or aerosol and cloud chemistry, for which current GEOS-Chem treatments are documented in Holmes et al. (2019); Shah et al. (2020); Wang et al. (2021). A total of 63 gas-phase thermal reactions (out of the 650 in GEOS-Chem version 14.0.1, in addition to 157 photolyses and 107 aerosol and cloud reactions) are updated with new rate coefficients and/or product distributions, including one newly added reaction. Table 1 lists the reactions updated with the old and the new rate coefficients and products given, and Figures S1-S9 in the supplementary

55 material show the impact of these updates on rate coefficients as a function of temperature and/or pressure. The following paragraphs provide a summary of the changed rate coefficients and product yields, organized by chemical family as in Table 1. All updates are from the JPL Data Evaluation unless otherwise noted.

Eleven updated reaction rate coefficients correspond to inorganic reactions in the reactive nitrogen (NO_y = NO + NO_2 + all oxidized odd nitrogen species) family, with new values derived predominantly from changes to the methods of combining

60 data from previous studies. Most notable among these updates is a reversal in the temperature dependence from positive to negative for the reaction between nitrous acid (HONO) and OH, resulting in a 40% increase in the rate coefficient at 300 K rising to a 300% increase at 200 K. The new assessment prioritizes the temperature dependence measured by Burkholder et al. (1992) over that of Jenkin and Cox (1987), which had previously been used. Rate coefficient formulas for the two pressure- and temperature-dependent branches of the O + NO_2 reaction – association to yield NO_3 and activation to yield NO + O_2 – were

65 rebalanced, resulting in increases to the former branch of 19-21% and a decrease to the latter of 10-18% (producing an overall decrease of 6-9%) under typical conditions between altitudes of 0 km (288 K, 1013 hPa) and 10 km (240 K, 270 hPa). The combined termolecular activation and association reactions of OH + HNO_3, both yielding NO_3 + H_2O, were also reanalyzed based on new experimental work by Winiberg et al. (2018) and Dulitz et al. (2018), resulting in changes to its rate coefficient of -1% to +4% over the range of atmospheric conditions. Other updates in this family include a rate coefficient increase for

70 NO_3 + O (+30%) and decreases for OH + NO_3 (-9%) and NO_2 + NO_3 (-33% – -25% over the range 200–300 K); weaker temperature dependencies and adjusted rate constants for HO_2 + NO, NO + NO_3, and N + O_2, resulting in changes to their coefficients over the range 200–300 K of -1% – +1%, -10% – -2%, and +109% – -1% respectively; and a stronger temperature dependence for OH + HNO_4 (+9% – -25%).

Thirteen of the changes are updates to branching ratios in reactions of O^1D with HBr, HCl, and halogenated organic com-

75 pounds. These adjustments are generally minor, shifting the branching between the O + XR and OX + R product channels (where X stands in for Cl or Br and R stands in for H or an organic group) by a few percent. We also add the newly included O^1D + CH_3Cl reaction and update the temperature dependencies of the O^1D + CFC114 and O^1D + CFC115 reactions to the JPL recommendations based on Baasandorj et al. (2013), resulting in increases of between 18% and 35% to their rate coefficients over the range 200–300 K.

80 Four updates apply to the rate coefficients of organic ozonolysis reactions. While three of these (O_3 + ethene, propene, and methacrolein) are only small adjustments to temperature dependence, resulting in rate coefficient increases of 2–12% over the range 200–300 K, the isoprene ozonolysis reaction in GEOS-Chem did not previously have a temperature dependence. We include that now per JPL recommendation, which considerably slows ozonolysis at low temperatures (-96% at 200 K, -44% at 273 K) and accelerates it when T > 297 K.

85 Ten rate coefficients of OH + organic reactions are changed – five based on JPL recommendations and five from IUPAC. From JPL, the notable update is to the two C_3H_8 + OH branches (primary and secondary abstraction). The two branches have different temperature dependencies, a feature which had previously been included in GEOS-Chem, but the reanalysis in this JPL Data Evaluation changes both dependencies considerably, reversing the dependence of the secondary abstraction. Overall, the importance of secondary abstraction branch increases; its rate coefficient goes up 300% at 200 K but barely changes at

90   300, while the primary goes up 140% at 200 but drops 30% at 300. (This is after accounting for the apparent typo in the primary abstraction rate constant from the JPL Data Evaluation, which would increase its rate coefficient by a factor of 10). The other JPL-derived revisions include a reduction in the OH oxidation rate coefficient for C_{3+} alcohols ("ROH") by 4% and weaker temperature dependencies for OH + CH_2Cl_2 and CH_3Cl, changing their rate coefficients by +2% – -9% and +37% – -3% respectively over the temperature range 200–300 K. The IUPAC-derived updates include the addition of a temperature

95   dependence for the methylglyoxal + OH reaction based on Baeza-Romero et al. (2007) and Tyndall et al. (1995), changing its rate coefficient by +125% at 200 K and -14% at 300 K; minor changes to the temperature dependencies of the methyl ethyl ketone + OH rate coefficient (-17% – -7% at 200–300 K) and to both branches of the hydroxyacetone + OH reaction (0% – -2%), and a factor of 30-50 downward revision to the OH + peroxyacetic acid (PAA) rate coefficient based on the experimental and theoretical results of Berasategui et al. (2020).

100   Five rate coefficients of reactions between the Cl radical and organic compounds are updated. The Cl + acetone rate coefficient now has a smaller temperature dependence and faster rate at temperatures below 251 K, resulting in a slower reaction by 22% at 300 K but a faster reaction by 49% at 200 K than previously. The Cl + CH_2O reaction has the same temperature dependence, but its rate constant is revised upward by 11%. The other three changes are to Cl + chloromethane compounds; the Cl + CH_2Cl_2 rate constant, though unchanged in Publication 19-5 from previous JPL data evaluations, may have been

105   erroneously low in GEOS-Chem, because we find it requires increasing by a factor of 10.2–13.3 over the range 200–300 K to match the recommendation. The updates to the Cl + CH_3Cl and Cl + $CHCl_3$ coefficients are much smaller, changing by +3% – 0% and -3% – -6% respectively over the range 200–300 K.

    Five revisions apply to reactions of organic peroxy (RO_2) radicals, including increases in the rate coefficients of the self reaction of the peroxyacetyl radical (CH_3CO_3) by 14%, the reaction of NO with the acetone-derived peroxy radical

110    $CH_3C(O)CH_2O_2$ by 4%, the reaction of the ethylperoxy radical ($CH_3CH_2O_2$) with HO_2 (+1%), and other functionalized C_2 peroxy radicals + HO_2 (+1%). These updates also include a slight increase in the temperature- and pressure-dependent peroxyacetyl nitrate (PAN) formation rate (the termolecular reaction of CH_3CO_3 + NO_2) by about 2% under typical conditions between altitudes of 0 km (288 K, 1013 hPa) and 10 km (240 K, 270 hPa). However, the PAN equilibrium remains unchanged in this JPL assessment, so we also adjust the dissociation reaction rate coefficient accordingly.

115   Four updates pertain to the fates of Criegee Intermediates. Some of these reactions are newly included in the JPL Data Evaluation, and had previously received scant attention in GEOS-Chem; they were generally added selectively to the mechanism either to provide a source of HCOOH (Millet et al., 2015) or to complete the isoprene oxidation cascade (Bates and Jacob, 2019). Updates include substantial increases in the rate coefficients of CH_2OO + NO_2 (+4250%) and CH_3CHOO + SO_2 (+377%), a slight increase to CH_2OO + SO_2 (+3%), and a sharp decrease to the rate coefficient of CH_2OO + H_2O (-84%).

120   Six changes are made to reactions in the iodine radical chemistry scheme, most notably a downward revision by 54% to the IO + ClO rate constant. The temperature dependence of the IO + BrO reaction is increased, resulting in changes to its rate coefficient of +28% at 200 K ranging to -16% at 300 K. Conversely, temperature dependencies are weakened for the IO + NO and I + O_3 reactions, resulting in changes of +6% – -1% and -10% – -9% respectively over the range 200-300 K. Slight adjustments to the I + NO and I + NO_2 rate coefficients result in decreases of <1% and <3% respectively.

125 Five other miscellaneous rate coefficient changes complete the list. First, a revision to the formula for the termolecular reaction of SO_2 with OH results in pressure- and temperature-dependent rate coefficient decreases of 0–5% under typical conditions between altitudes of 0 km (288 K, 1013 hPa) and 10 km (240 K, 270 hPa). Similar revisions to the formula for the termolecular $H + O_2$ reaction and the combined activation and association reactions of OH + CO result in rate coefficient increases under the same range of atmospheric conditions of 23–34% and 3-5% respectively. Finally, a weaker temperature

130 dependence for the reaction of OCS with OH renders the rate coefficient nearly unchanged at 300 K but 10% faster at 250 K and 25% faster at 200 K.

The product distributions of a further 63 reactions listed in Table S2 were adjusted so as to balance carbon and nitrogen between the reactants and products. Previously, CO_2 had not explicitly been represented as a product in many reactions, while others were imbalanced due to rounding errors or uncertainties in product branching ratios. The updated reactions were

135 balanced predominantly by adding CO_2 as a coproduct, adjusting branching ratios slightly to offset rounding errors, or adding lumped organic products (e.g. "RCHO" for C_{3+} aldehydes, which carries 3 carbon atoms) to account for products whose specific structure is unknown. There remain 54 reactions (Table S3) that are imperfectly carbon- or nitrogen-balanced; most are (a) in the monoterpene oxidation submechanism (Fisher et al., 2016); (b) reactions of (H)CFCs, which play a minor role in the atmospheric carbon budget; and (c) reactions coupling the gas-phase organic mechanism to the formation of non-specific

140 particle-phase species (e.g., a single aerosol-phase isoprene-derived nitrate species carries five carbons and one nitrogen, but is formed via uptake of species with 4-5 carbons and 1-2 nitrogens). Balancing these reactions will be the focus of future efforts.

Table 1: GEOS-Chem reactions updated per JPL and IUPAC recommendations[a]

Reactants	Products (old mechanism)	Rate coefficient[b] (old mechanism)	New rate coefficient[b] and/or products
NO_y reactions			
OH + NO_3	$HO_2 + NO_2$	2.2×10^{-11}	2.0×10^{-11}
$NO_2 + NO_3$	$NO + NO_2 + O_2$	$4.5 \times 10^{-14} \times e^{-1260/T}$	$4.35 \times 10^{-14} \times e^{-1335/T}$
$O + NO_3$	$NO_2 + O_2$	1.0×10^{-11}	1.3×10^{-11}
$OH + HNO_2$	$NO_2 + H_2O$	$1.8 \times 10^{-11} \times e^{-390/T}$	$3.0 \times 10^{-12} \times e^{250/T}$
$OH + HNO_4$	$NO_2 + O_2 + H_2O$	$1.3 \times 10^{-12} \times e^{380/T}$	$4.5 \times 10^{-13} \times e^{610/T}$
$HO_2 + NO$	$OH + NO_2$	$3.3 \times 10^{-12} \times e^{270/T}$	$3.44 \times 10^{-12} \times e^{260/T}$
$N + O_2$	$NO + O$	$1.5 \times 10^{-11} \times e^{-3600/T}$	$3.3 \times 10^{-12} \times e^{-3150/T}$
$NO + NO_3$	$2 NO_2$	$1.5 \times 10^{-11} \times e^{170/T}$	$1.7 \times 10^{11} \times e^{125/T}$
$OH + HNO_3$ [+ M]	$NO_3 + H_2O$ [+ M]	$f_x(2.41e-14,2.69e-17,6.51e-34)^c$	$f_a(3.9e-31,7.2,1.5e-13,4.8,3.7e-14,-240)^c$
$O + NO_2$	$NO + O_2$	$5.1 \times 10^{-12} \times e^{210/T}$	$f_b(3.4e-31,1.6,2.3e-11,0.2,5.3e-12,-200)^c$
$O + NO_2$ [+ M]	NO_3 [+ M]	$f_t(2.5e-31,1.8,2.2e-11,0.7)^c$	$f_t(3.4e-31,1.6,2.3e-11,0.2)^c$
O^1D-halogen reactions			
$O^1D + HCl$	0.67(Cl + OH) + 0.24(ClO + H) + 0.09(HCl + O)	1.5×10^{-10}	0.66(Cl + OH) + 0.22(ClO + H) + 0.12(HCl + O)
$O^1D + HBr$	0.65(Br + OH) + 0.2(HBr + O) + 0.15(BrO + H)	1.5×10^{-10}	0.6(Br + OH) + 0.2(HBr + O) + 0.2(BrO + H)
$O^1D + CHBr_3$	1.36 Br + 0.68 BrO + 0.32($CHBr_3$ + O)	6.6×10^{-10}	1.4 Br + 0.7 BrO + 0.3($CHBr_3$ + O)

Continued on next page

Reactants	Products (old mechanism)	Rate coefficient[b] (old mechanism)	New rate coefficient[b] and/or products
$O^1D + CCl_4$	$2.58\ Cl + 0.86\ ClO + 0.14(CCl_4 + O)$	3.3×10^{-10}	$2.37\ Cl + 0.79\ ClO + 0.21(CCl_4 + O)$
$O^1D + CFC11$	$1.76\ Cl + 0.88\ ClO + 0.12(CFC11 + O)$	2.3×10^{-10}	$1.8\ Cl + 0.9\ ClO + 0.1(CFC11 + O)$
$O^1D + CFC113$	$1.5\ Cl + 0.75\ ClO + 0.25(CFC113 + O)$	2.32×10^{-10}	$1.8\ Cl + 0.9\ ClO + 0.1(CFC113 + O)$
$O^1D + CFC114$	$0.75(Cl + ClO) + 0.25(CFC114 + O)$	$1.3 \times 10^{-10} \times e^{-25/T}$	$1.3 \times 10^{-10} \times e^{25/T}$; $0.95\ Cl + 0.85ClO + 0.1(CFC114 + O)$
$O^1D + CFC115$	$0.7(CFC115 + O) + 0.3\ ClO$	$5.4 \times 10^{-11} \times e^{-30/T}$	$5.4 \times 10^{-11} \times e^{30/T}$; $0.86\ ClO + 0.14(CFC115 + O)$
$O^1D + HCFC22$	$0.55\ ClO + 0.28(HCFC22 + O) + 0.17\ Cl$	1.02×10^{-10}	$0.56\ ClO + 0.25(HCFC22 + O) + 0.19\ Cl + 0.05\ OH$
$O^1D + HCFC142b$	$0.74\ ClO + 0.26(HCFC142b + O)$	2.0×10^{-10}	$0.65\ ClO + 0.35(HCFC142b + O)$
$O^1D + H1211$	$0.36(H1211 + O) + 0.33(ClO + Br) + 0.31(Cl + BrO)$	1.5×10^{-10}	$0.35(H1211 + O) + 0.34(ClO + Br) + 0.31(Cl + BrO)$
$O^1D + H1301$	$0.59(H1301 + O) + 0.41\ BrO$	1.0×10^{-10}	$0.55(H1301 + O) + 0.45\ BrO$
$O^1D + CH_3Cl$	N/A	N/A	2.6×10^{-10}; $0.9\ CH_3OO + 0.46\ ClO + 0.35\ Cl + 0.1(O + CH_3Cl) + 0.09\ H$
Ozonolysis reactions			
Ethene + O_3	$CH_2O + CH_2OO$	$9.1 \times 10^{-15} \times e^{-2580/T}$	$1.2 \times 10^{-14} \times e^{-2630/T}$
Propene + O_3	$0.5\ CH_3CHO + 0.5\ CH_2O + ...$	$5.5 \times 10^{-15} \times e^{-1880/T}$	$6.5 \times 10^{-15} \times e^{-1900/T}$
Methacrolein + O_3	$0.88\ CH_3C(O)CHO + ...$	$1.4 \times 10^{-15} \times e^{-2100/T}$	$1.5 \times 10^{-15} \times e^{-2110/T}$
Isoprene + O_3	$0.827\ CH_2O + 0.58\ CH_2OO + ...$	1.3×10^{-17}	$1.1 \times 10^{-14} \times e^{-2000/T}$
OH + organic reactions			
Propane + OH	$CH_3CH(OO)CH_3$	$f_P(5.87,0.64,-816)^c$	$8.54 \times 10^{-13} \times e^{-19/T} \times (\frac{298}{T})^{1.54}$
Propane + OH	$CH_3CH_2CH_2OO$	$f_P(0.17,-0.64,816)^c$	$1.97 \times 10^{-12} \times e^{-675/T} \times (\frac{298}{T})^{1.23}$
C_{3+} alcohol + OH	C_{3+} aldehyde + HO_2	$4.6 \times 10^{-12} \times e^{70/T}$	$4.4 \times 10^{-12} \times e^{70/T}$
$CH_2Cl_2 + OH$	$2\ Cl + HO_2$	$2.61 \times 10^{-12} \times e^{-944/T}$	$1.92 \times 10^{-12} \times e^{-880/T}$
$CHCl_3 + OH$	$3\ Cl + HO_2$	$4.69 \times 10^{-12} \times e^{-1134/T}$	$2.2 \times 10^{-12} \times e^{-920/T}$
$CH_3C(O)CHO + OH$	$CH_3CO_3 + CO$	1.5×10^{-11}	[d] $1.9 \times 10^{-12} \times e^{575/T}$
$CH_3C(O)CH_2CH_3 + OH$	$CH_3C(O)CH_2CH_2OO$	$1.3 \times 10^{-12} \times e^{-25/T}$	[d] $1.5 \times 10^{-12} \times e^{-90/T}$
$CH_3CO_3H + OH$	CH_3CO_3	$6.13 \times 10^{-13} \times e^{200/T}$	[d] 3.0×10^{-14}; $0.78\ CH_3CO_3 + 0.22(OH + CO_2 + CH_2O)$
$CH_3C(O)CH_2OH + OH$	$CH_3C(O)CHO + HO_2$	$f_{HA}(2.15e\text{-}12,305)^c$	[d] $f_{HA}(2.0e\text{-}12,320)^c$
$CH_3C(O)CH_2OH + OH$	$0.5(CH_3CO_2H + HCOOH) + ...$	$f_{HB}(2.15e\text{-}12,305)^c$	[d] $f_{HB}(2.0e\text{-}12,320)^c$
Cl + organic reactions			
$Cl + CH_2O$	$CO + HCl + HO_2$	$7.32 \times 10^{-11} \times e^{-30/T}$	$8.1 \times 10^{-11} \times e^{-30/T}$
Cl + Acetone	$HCl + CH_3C(O)CH_2OO$	$7.7 \times 10^{-11} \times e^{-1000/T}$	$1.63 \times 10^{-11} \times e^{-610/T}$
$Cl + CH_3Cl$	$CO + 2\ HCl + HO_2$	$2.17 \times 10^{-11} \times e^{-1130/T}$	$2.03 \times 10^{-11} \times e^{-1110/T}$
$Cl + CH_2Cl_2$	$CO + HCl + HO_2 + 2\ Cl$	$1.24 \times 10^{-12} \times e^{-1070/T}$	$7.4 \times 10^{-12} \times e^{-910/T}$
$Cl + CHCl_3$	$CO + HCl + HO_2 + 3\ Cl$	$3.77 \times 10^{-12} \times e^{-1011/T}$	$3.3 \times 10^{-12} \times e^{-990/T}$
Peroxy radical (RO_2) reactions			
$CH_3CO_3 + CH_3CO_3$	$2\ CH_3OO$	$2.5 \times 10^{-12} \times e^{500/T}$	$2.9 \times 10^{-12} \times e^{500/T}$
$CH_3C(O)CH_2OO + NO$	$CH_3CO_3 + CH_2O + NO_2$	$2.8 \times 10^{-12} \times e^{300/T}$	$2.9 \times 10^{-12} \times e^{300/T}$
$CH_3CH_2OO + HO_2$	CH_3CH_2OOH	$7.4 \times 10^{-13} \times e^{700/T}$	$7.5 \times 10^{-13} \times e^{700/T}$

Reactants	Products (old mechanism)	Rate coefficient[b] (old mechanism)	New rate coefficient[b] and/or products
OTHRO2[e] + HO$_2$	CH$_3$CH$_2$OOH	$7.4 \times 10^{-13} \times e^{700/T}$	$7.5 \times 10^{-13} \times e^{700/T}$
CH$_3$CO$_3$ + NO$_2$ [+ M]	PAN [+ M]	$f_t(9.7e\text{-}29,5.6,9.3e\text{-}12,1.5)^c$	$f_t(7.3e\text{-}29,4.1,9.5e\text{-}12,1.6)^c$
Criegee Intermediate reactions			
CH$_2$OO + NO$_2$	CH$_2$O + NO$_3$	1.0×10^{-15}	4.25×10^{-12}
CH$_2$OO + SO$_2$	CH$_2$O + SO$_4$	3.7×10^{-11}	3.8×10^{-11}
CH$_2$OO + H$_2$O	0.73 HMHP + 0.21 HCOOH + ...	1.7×10^{-15}	2.8×10^{-16}
CH$_3$CH$_2$OO + SO$_2$	CH$_3$CHO + SO$_4$	7.0×10^{-14}	2.65×10^{-11}
Iodine reactions			
IO + NO	I + NO$_2$	$9.1 \times 10^{-12} \times e^{240/T}$	$8.6 \times 10^{-12} \times e^{230/T}$
IO + ClO	0.801 I + 0.56 OClO + ...	$8.93 \times 10^{-12} \times e^{280/T}$	$4.82 \times 10^{-12} \times e^{280/T}$
IO + BrO	Br + 0.8 OIO + ...	$1.5 \times 10^{-11} \times e^{510/T}$	$5.5 \times 10^{-12} \times e^{760/T}$
I + O$_3$	IO + O$_2$	$2.3 \times 10^{-11} \times e^{-870/T}$	$2.0 \times 10^{-11} \times e^{-830/T}$
I + NO [+ M]	INO [+ M]	$f_t(1.8e\text{-}32,1,1.77e\text{-}11,0)^c$	$f_t(1.8e\text{-}32,1,1.7e\text{-}11,0)^c$
I + NO$_2$ [+ M]	IONO [+ M]	$f_t(3e\text{-}31,1,6.6e\text{-}11,0,0.63)^c$	$f_t(3e\text{-}31,1,6.6e\text{-}11,0,0.6)^c$
Other reactions			
OCS + OH	CO$_2$ + SO$_2$	$1.1 \times 10^{-13} \times e^{-1200/T}$	$7.2 \times 10^{-14} \times e^{-1070/T}$
CO + OH [+ M]	HO$_2$ + CO$_2$ [+ M]	$f_c(5.9e\text{-}33,1.1e\text{-}12,1.5e\text{-}13,2.1e9)^c$	$f_a(6.9e\text{-}33,2.1,1.1e\text{-}12,-1.3,1.85e\text{-}13,65)^c$
SO$_2$ + OH [+ M]	SO$_4$ + HO$_2$ [+ M]	$f_t(3.3e\text{-}31,4.3,1.6e\text{-}12,0)^c$	$f_t(2.9e\text{-}31,4.1,1.7e\text{-}12,-0.2)^c$
H + O$_2$ [+ M]	HO$_2$ [+ M]	$f_t(4.4e\text{-}32,1.3,7.5e\text{-}11,-0.2)^c$	$f_t(5.3e\text{-}32,1.8,9.5e\text{-}11,-0.4)^c$
PAN [+ M]	CH$_3$CO$_3$ + NO$_2$ [+ M]	$f_d(9.7e\text{-}29,5.6,9.3e\text{-}12,1.5)^c$	$f_d(7.3e\text{-}29,4.1,9.5e\text{-}12,1.6)^c$

[a] Updates are from JPL Data Evaluation recommendations unless denoted otherwise by a table footnote in Column 4; GEOS-Chem names for chemical species listed here by formula or common name are given in Table S1; [b] In units cm^3 molecule^{-1} s^{-1} unless otherwise noted; T is temperature in K. [c] Formulas for the rate coefficients of propane + OH (f_P), hydroxyacetone + OH (f_{HA} & f_{HB}), termolecular reactions (f_t), dissociations (f_d, units s^{-1}), activation reactions (f_a & f_b), and previous GEOS-Chem parameterizations of OH + HNO$_3$ (f_x) and OH + CO (f_c) are given in Section S1; [d] Per IUPAC recommendations; [e] OTHRO2 represents functionalized C$_2$ peroxy radicals aside from CH$_3$CH$_2$OO.

3   Model simulations

We use version 14.0.1 of GEOS-Chem Classic (DOI: 10.5281/zenodo.7271974) driven by NASA MERRA-2 assimilated meteorological data to simulate the impacts of the updated rate coefficients on trace gas concentrations and budgets. Detailed gas and aerosol chemistry is computed throughout the troposphere and stratosphere at 30 minute time intervals using a fourth-order Rosenbrock kinetic solver implemented with the Kinetic PreProcessor (KPP) version 3.0 (Lin et al., 2023). Emissions are calculated at 30 minute time steps using the Harmonized Emissions Component (HEMCO) version 3.0 (Lin et al., 2021). This includes anthropogenic emissions from the Community Emissions Data System (CEDS) inventory (Hoesly et al., 2018), biomass burning emissions from the Global Fire Emissions Database (GFED) version 4 (van der Werf et al., 2017), and biogenic VOC emissions from the Model of Emissions of Gases and Aerosols from Nature (MEGAN) version 2.1 (Guenther et al., 2012) as implemented by Hu et al. (2015) and calculated offline to improve reproducibility across scales (Weng et al., 2020). Additional emission sources, including air-sea exchange of organics, NO$_x$ (NO + NO$_2$) from soils and lightning, and others,

follow the default GEOS-Chem version 14.0 settings. Methane is treated as an advected and reactive species, but without
emissions; instead, surface concentrations are prescribed based on measured monthly means (Murray, 2016).

To calculate the changes in burdens and budgets of atmospheric species described in the following section, we perform two
simulations: one with the unchanged chemical mechanism from GEOS-Chem classic version 14.0.1 ("base") and another with
the mechanism altered to include the updates listed in Tables 1, S2, and S4 ("updated"). Both simulations are performed at
$2° \times 2.5°$ horizontal resolution over 72 vertical levels, are initialized from the same generic concentration fields that reflect
realistic atmospheric concentrations of model species, and are run for two years (1 January 2017 to 1 January 2019). The
first year is to remove the effect of the common initialization. We use output from the second year to compute the changes
described below. While this spinup is sufficient to demonstrate direct changes to most species concentrations from updated rate
coefficients and product yields, it does not reflect effects of longer-term processes like stratosphere-troposphere exchange.

4 Impacts on species concentrations

Figures 1-5 show the impacts of the rate coefficient and product yield updates on annually averaged surface mixing ratios,
zonally averaged mixing ratios, and total tropospheric and stratospheric burdens of selected species. These changes are also
described and explained in the following paragraphs. A more complete list of impacts on annually averaged tropospheric mass
burdens for all species in GEOS-Chem that change by >1% can be found in Table S5, and a similar list for stratospheric changes
can be found in Table S6.

Figure 1 shows the effects of the mechanism changes on ozone, HO_x (= OH + HO_2), and H_2O_2. Total tropospheric ozone
decreases by 0.7% in the updated mechanism, corresponding to a surface decrease of 0.5 ppb in the extratropics, driven in part
by reduced PAN-driven NO_x transport (described below) and in part by faster organic ozonolysis reactions. Over East Asia,
where faster CO + OH and C_3H_8 + OH reactions increase radical cycling, and tropical forests, where isoprene ozonolysis is
slowed and NO_x is increased due to better nitrogen conservation in the reaction forming methyl vinyl ketone hydroxynitrate
(MVKN), surface ozone rises by 0.1-0.3 ppb. The upper troposphere and mid stratosphere both experience much stronger ozone
decreases of up to 5% in the extratropics, due respectively to lower NO_x-driven formation and higher NO_x-driven catalytic
losses. These reductions are partially balanced by an ozone increase at 50-100 hPa driven by the updated N + O_2 reaction,
leading to a net decrease of only 0.7% in stratospheric ozone.

In contrast to the decreased ozone, tropospheric HO_x and H_2O_2 burdens all increase slightly (OH +0.3%, HO_2 +1.0%,
H_2O_2 +1.3%). Increased tropospheric OH is driven largely by the reduced PAA + OH rate coefficient, particularly in the up-
per troposphere, which is partially offset by the changes to CO + OH and HNO_z + OH rate coefficients. Higher OH leads to
increases in the methane loss rate, causing an overall 0.4% decrease in the methane lifetime against oxidation by tropospheric
OH. Higher tropospheric HO_2 and H_2O_2 are driven largely by the accelerated CO + OH rate, with stronger increases in the
upper troposphere due to changes in OH + HNO_z (z=2–4) and over regions with strong biogenic influence due to the revised
nitrogen conservation from MVKN. Higher HO_2 over forests increases the proportion of isoprene-derived peroxy radicals
reacting with HO_2, which correspondingly decreases the fraction that react via the OH-recycling isomerization channel, re-

ducing OH over the Amazon (-1%) and the tropospheric burdens of organic products from the isomerization pathway (e.g. C_5 hydroperoxyaldehydes, -2.2%).
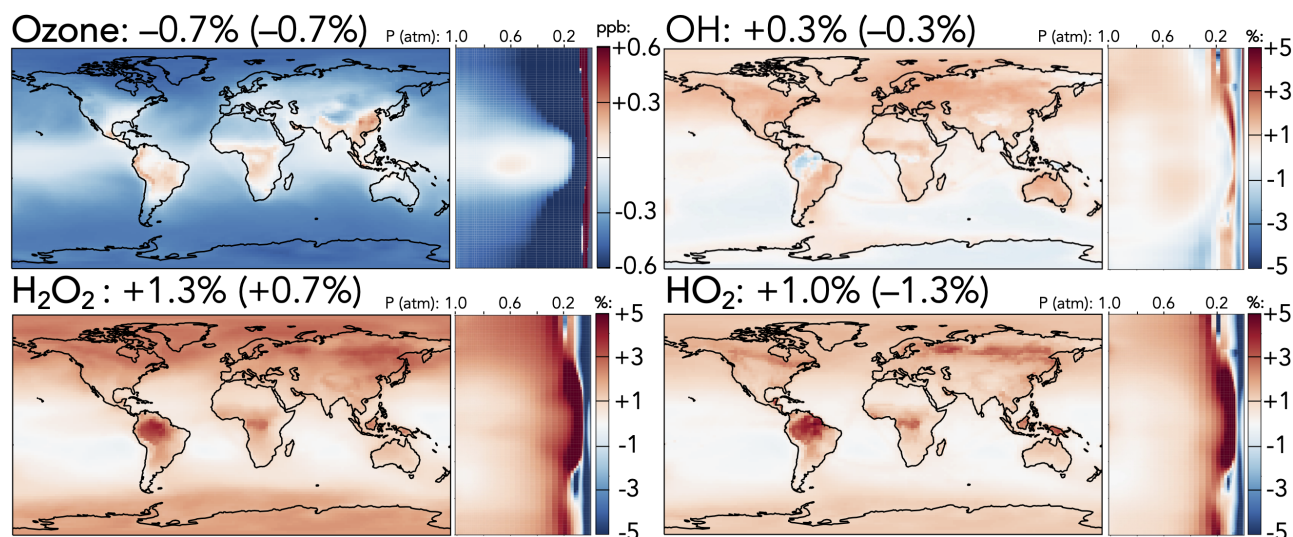
Figure 1. Absolute (top left, for ozone) and relative (all others) changes in the annual average mixing ratios of $(H)O_y$ species between the base and updated mechanism. Maps show surface values; atmospheric cross-sections show zonal means using the labelled altitude scale and the same latitude scales as the maps to their left. Additional vertical profiles of these species' changes can be found in Figure S12 in the supplementary material. Scales differ between species but are the same for each individual species' surface maps and cross-sections. Numbers next to species names show the percent change in their annual average tropospheric burden (stratospheric burden in parentheses) from the base to the updated mechanism.

The cumulative effects of the changes in reactive nitrogen species are shown in Figure 2, including the absolute change in
190   NO_x from the base to the updated mechanism (top left) and relative changes for individual species. Maps of absolute changes of the other NO_y species, which tend to highlight differences in NO_x-rich areas with high anthropogenic influence, are shown in Figure S11. The net effect of the updates on the tropospheric NO_x burden is a 1.7% decrease, with a stronger reduction of NO (-2.4%) than NO_2 (-1.0%). This decrease is dominated by annual average reductions of over 25 ppt over China and the Indo-Gangetic Plain as well as in the tropical upper troposphere, slightly offset by surface NO_x increases of 1-10 ppt in
195   low-NO_x regions such as the Amazon and high-latitude oceans. Both NO and NO_2 exhibit strong stratospheric increases (+8% and +7% respectively), driven in the upper stratosphere by weaker NO_x loss from a higher $N + O_2$ rate coefficient (N originates from NO photolysis and the $N + O_2$ reaction returning NO competes with $N + NO$ producing N_2) and in the lower stratosphere by changes to the $HNO_z + OH$ reactions.

Other NO_y species generally exhibit changes directly attributable to updates in their own sources or sinks. NO_3, for which
200   loss rate coefficients to reactions with NO_x and OH are revised downward and the stratospheric source from $O + NO_2$ is revised upward, generally increases at the surface (up to +0.5 ppt in India and China) and in the stratosphere (+0.4%), although
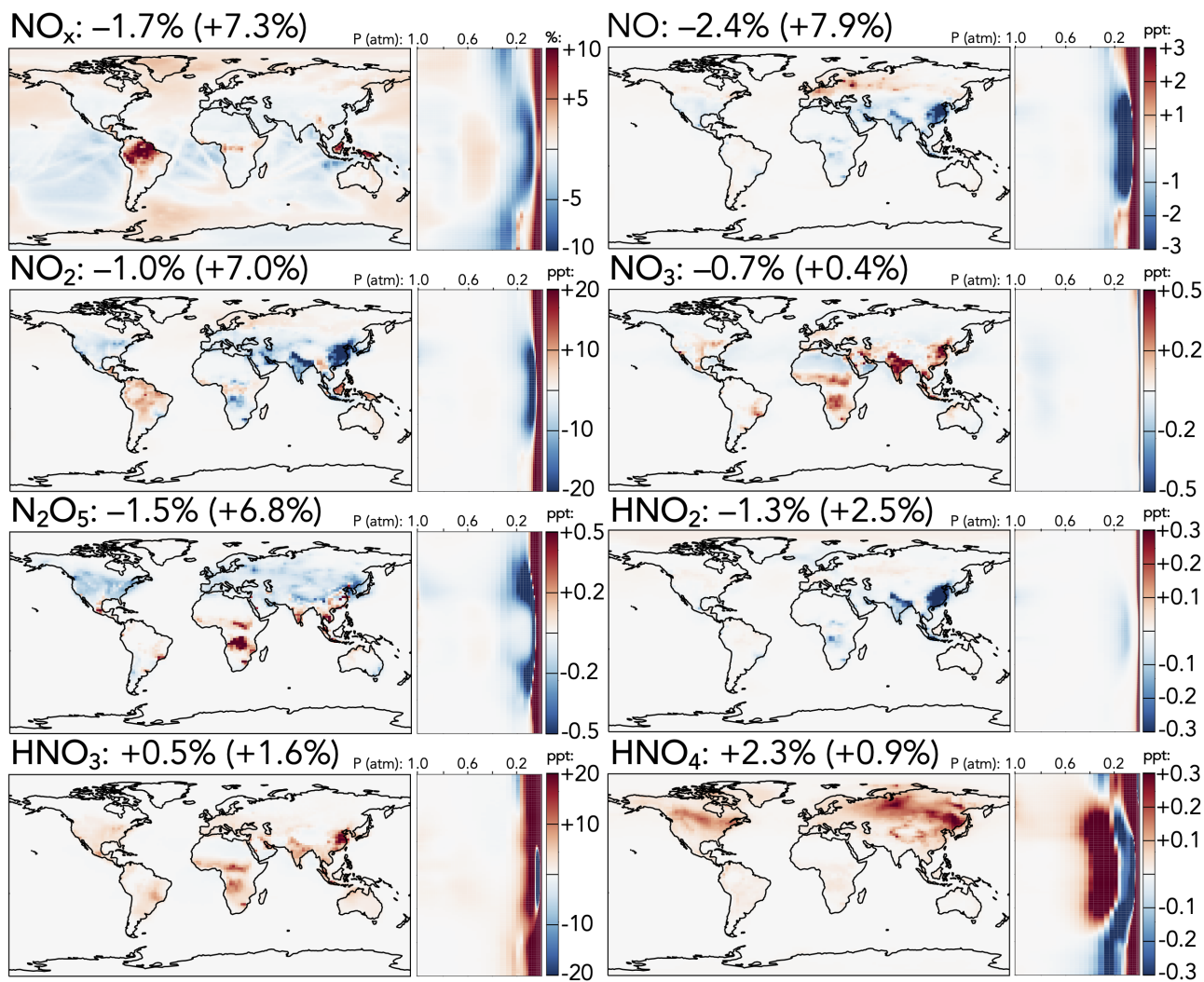
Figure 2. Absolute (top left, for NO_x) and relative (all others) changes in the annual average mixing ratios of NO_y species between the base and updated mechanism. Maps show surface values; atmospheric cross-sections show zonal means using the labelled altitude scale and the same latitude scales as the maps to their left. Additional vertical profiles of these species' changes can be found in Figure S13 in the supplementary material. Scales differ between species but are the same for each individual species' surface maps and cross-sections. Numbers next to species names show the percent change in their annual average tropospheric burden (stratospheric burden in parentheses) from the base to the updated mechanism.

this is offset by a decrease in the mid-troposphere. The stratospheric NO_3 increase is not nearly as strong as that of NO_x, potentially due to faster loss from the increased $O + NO_3$ rate coefficient and decreased formation via $O_3 + NO_2$ from the reduction in stratospheric ozone. Changes in N_2O_5 follow those of its precursors, NO_2 and NO_3, including a decrease of 1.5% in the troposphere and an increase of 6.8% in the stratosphere. Nitrous acid (HNO_2) is influenced both by changes to its

precursors (NO_x) and a decrease to its loss rate coefficient via reaction with OH; as a result, it decreases in the troposphere (-1.3%), especially over India and China where decreases to NO_x are strongest, and increases in the stratosphere (+2.5%). Nitric (HNO_3) and pernitric (HNO_4) acids increase slightly in both the troposphere and stratosphere, due to the combined effects of changes in their OH loss rate coefficients and in the mixing ratios of their major precursors.

210   Among C_1 species, whose changes are shown in Figure 3, two effects dominate: the increased CO + OH rate coefficient and the decreased C_1 stabilized Criegee Intermediate (CH_2OO) + H_2O rate coefficient. The former causes a 2.7% decrease in the tropospheric CO burden, corresponding to 1-2 ppb in the Southern Hemisphere and 2-3 ppb in the Northern Hemisphere, with smaller decreases at the continental surface where the change is partially offset by increased CO production from faster oxidation of volatile organics. The latter sharply reduces the formation of hydroxymethyl hydroperoxide (HMHP), the major

215 product of CH_2OO + H_2O, decreasing its tropospheric burden by 22%, with the strongest absolute effects (-50-75 ppt) over tropical and mid-latitude forests where the ozonolysis of biogenic emissions leads to high CH_2OO production. Formic acid, a product of the competing reaction of CH_2OO with the water dimer, increases accordingly by 3.1%. The tropospheric burdens of other C_1 species increase by 0.1-1.3% due to indirect effects of faster organic oxidation from the mechanism updates, with the strongest effects at the surface in regions of high biogenic influence and in the tropical upper troposphere.

220   Figure 4 shows the effects of the mechanism updates on selected larger organic species. Two effects dominate: the reduced PAA + OH rate coefficient and the rebalanced coefficients for primary versus secondary hydrogen abstract from propane by OH. The former leads directly to a 41% increase in the tropospheric PAA burden, with the strongest effects (+150%) in the upper troposphere where the longer PAA lifetime enables greater transport from lower-tropospheric source regions. Further, reduced regeneration of the peroxyacetyl radical (the product of PAA + OH) is compounded by an increase in its self-reaction

225 rate coefficient; as a result, the products of other peroxyacetyl radical reactions are all decreased, including PAN (-3.8%) and acetic acid (-3.4%). These reductions are enhanced by the updates to PAN cycling rate coefficients and the increased C_2 Criegee Intermediate + SO_2 coefficient, which decreases acetic acid formation via the competing C_2 Criegee Intermediate + H_2O reaction. The strongest relative effects of these changes (PAN -12%, acetic acid -6%) are over the tropical oceans, while their strongest absolute effects (-20 and -10 ppt respectively) are over tropical forests.

230   The adjusted propane oxidation mechanism causes a direct 17% decrease to the tropospheric propane burden due to the overall increased C_3H_8 + OH rate coefficient, as well as a number of knock-on effects from the increased proportion of secondary hydrogen abstraction relative to primary. Tropospheric burdens of the products of the peroxy radical from secondary abstraction all increase (i-propyl hydroperoxide +13%, i-propyl nitrate +8.6%, acetone +3.5%), while those from primary abstraction decrease (n-propyl hydroperoxide -4.3%, n-propyl nitrate -7.9%). Figure 4 shows the effects on acetone, the most

235 abundant and commonly measured of these products, but the spatial patterns of the other products are similar. While the relative changes in acetone burden (+4-8%) are evenly spread throughout the troposphere in the Northern Hemisphere, absolute changes are strongest over strong anthropogenic propane source regions (e.g. +200 ppt over East China). Products of acetone oxidation also exhibit enhancements; for example, the decrease in PAN mixing ratios from the updated PAA + OH coefficient is offset by the increase from higher acetone production, leading to minimal change in the northern extratropics, and the tropospheric

240 methylglyoxal burden increases by 1%. Methylglyoxal is also influence by the updated temperature dependence of its reaction
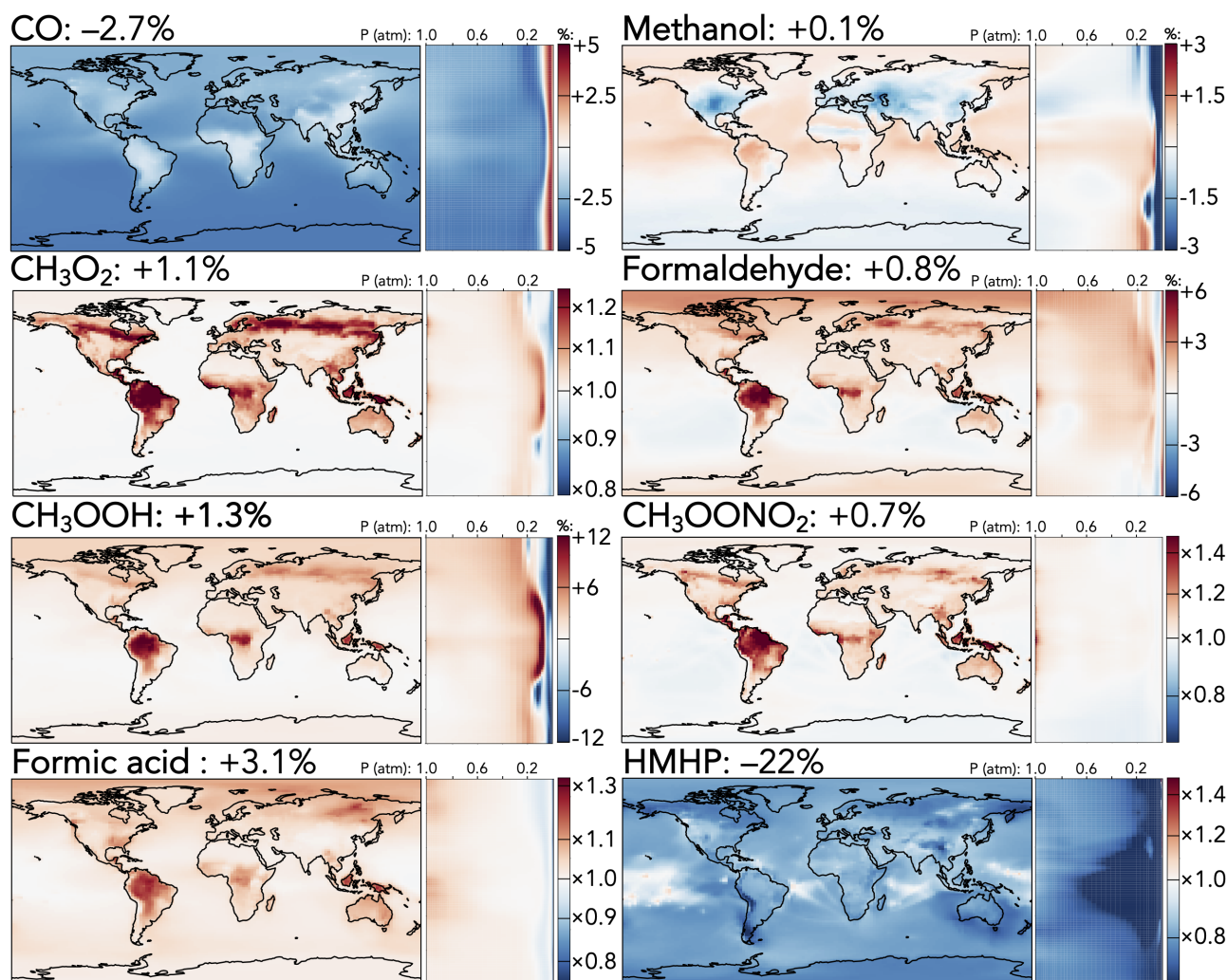
Figure 3. Relative changes in the annual average mixing ratios of C_1 species between the base and updated mechanism. Maps show surface values; atmospheric cross-sections show zonal means using the labelled altitude scale and the same latitude scales as the maps to their left. Additional vertical profiles of these species' changes can be found in Figure S14 in the supplementary material. Scales differ between species but are the same for each individual species' surface maps and cross-sections. Numbers next to species names show the percent change in their annual average tropospheric burden from the base to the updated mechanism.

with OH, leading to higher loss rates (and therefore lower mixing ratios) at colder temperatures, e.g. at high latitudes, and lower loss rates in the warmer tropics.

Finally, Figure 5 shows the effects of the mechanism updates on selected halogen radical species, which are dominated by changes to the participation of IO in the chlorine and bromine cycles. In general, the decreased IO + ClO rate coefficient leads 245 to higher chlorine reactivity via other pathways and a general increase in burdens of chlorine radical species; the tropospheric
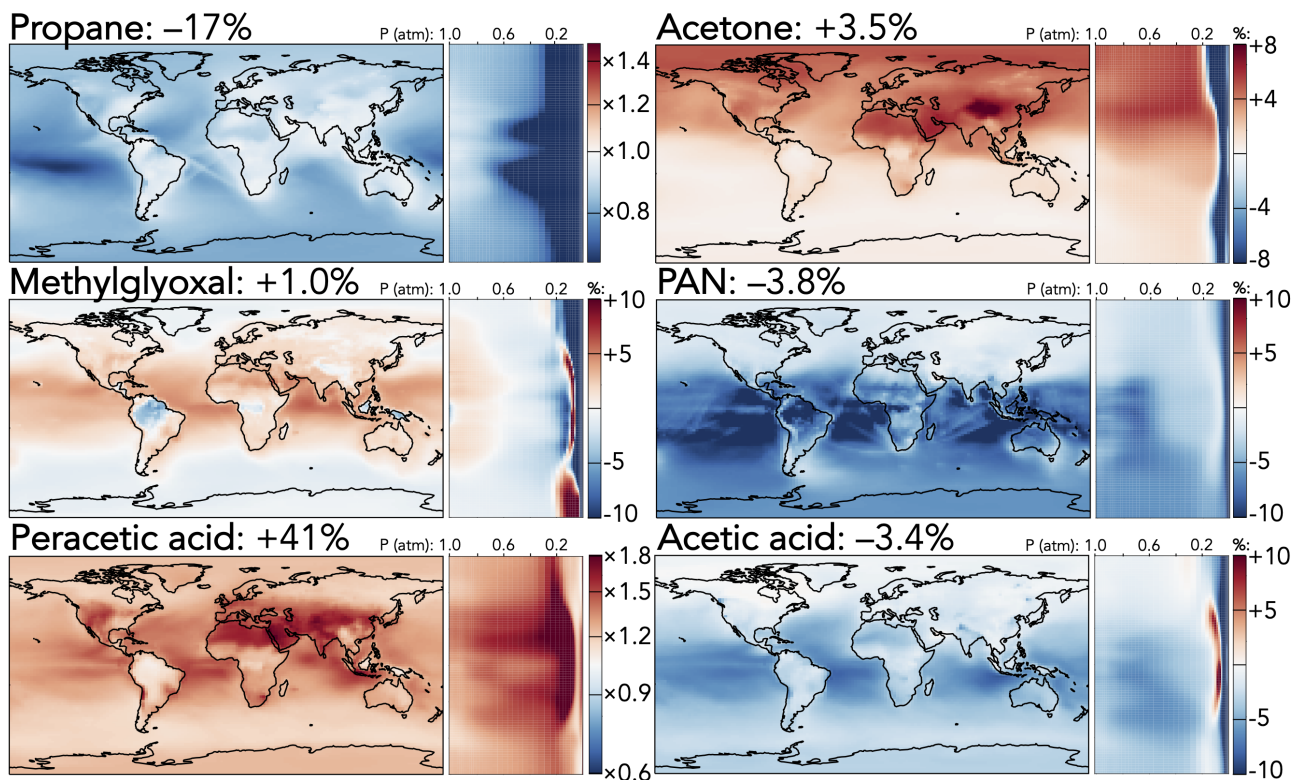
Figure 4. Relative changes in the annual average mixing ratios of select organic species between the base and updated mechanism. Maps show surface values; atmospheric cross-sections show zonal means using the labelled altitude scale and the same latitude scales as the maps to their left. Scales differ between species but are the same for each individual species' surface maps and cross-sections. Numbers next to species names show the percent change in their annual average tropospheric burden from the base to the updated mechanism.

burden of ClO rises by 4.1% and that of Cl_2O_2, the major product of ClO + ClO, by 27%, with the strongest effects in the upper troposphere and over the Antarctic. Other chlorine radical species exhibit smaller increases (Cl +1.4%, ClOO +3.0%) with similar spatial patterns, although OClO, a major product of IO + ClO, decreases (-0.7%). Effects in the stratosphere are similar except that ClO and Cl_2O_2 decrease, likely due to higher losses from increased NO_x.

250   In contrast to the effects on chlorine, iodine and bromine radical burdens are generally slightly decreased in the troposphere due both to the updated iodine chemistry with ClO/BrO/NO_x and to changes in NO_x distributions. Tropospheric burdens of most iodine species are moderately lower (I -1.5%, IO -0.3%, I_2O_4 -5.8%, INO -6.0%, IONO -9.2%), while those of bromine species are less affected (Br -0.6%, BrO -0.7%, $BrNO_2$ -2.9%, $BrNO_3$ -1.5%), although spatial variability due to adjusted temperature dependence and NO_x patterns lead to local changes of up to 3% in Br and BrO mixing ratios. In the stratosphere, 255   colder temperatures lead to an increase in the IO + BrO rate coefficient, causing the stratospheric BrO burden to decrease (-1.3%) and those of the IO + BrO products to increase (Br +1.0%, OIO +9.7%).
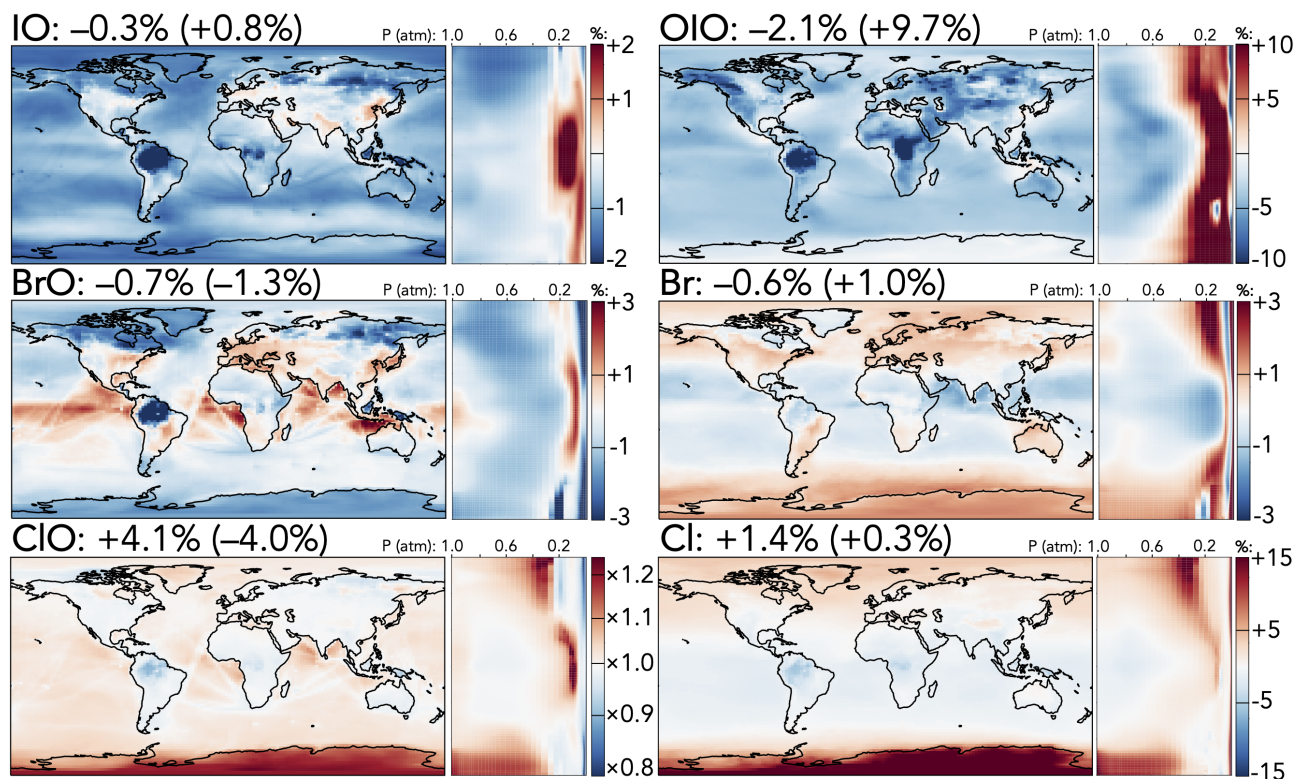
Figure 5. Relative changes in the annual average mixing ratios of select halogen species between the base and updated mechanism. Maps show surface values; atmospheric cross-sections show zonal means using the labelled altitude scale and the same latitude scales as the maps to their left. Additional vertical profiles of these species' changes can be found in Figure S15 in the supplementary material. Scales differ between species but are the same for each individual species' surface maps and cross-sections. Numbers next to species names show the percent change in their annual average tropospheric burden (stratospheric burden in parentheses) from the base to the updated mechanism.

Among the changes not shown in Figures 1-5, most are minor or are attributable to changes in carbon/nitrogen conservation (Table S2). Despite revisions to the rate coefficients of their reactions with OH, the atmospheric burdens of SO_2 and OCS barely change (+0.6% and -0.04% respectively). The addition of a strong temperature dependence to the isoprene ozonolysis rate coefficient also makes little difference; the tropospheric isoprene burden increases by 0.9%, and the decreased fraction of isoprene lost to ozonolysis contributes to the reduced HMHP described above. Most other volatile organic compounds exhibit slight decreases, likely due to the increase in tropospheric OH; for example, the tropospheric burdens of benzene, toluene, xylene, and lumped C_{4+} alkanes decrease by 0.5–0.6%. The effects on ethylene (-1.8%) and methacrolein (-2.1%) are enhanced by their increased ozonolysis rate coefficients. Carbon accounting changes cause larger increases to nonspecific C_{3+} organic products, e.g. RCHO (C_{3+} aldehydes; +7.4%), ROH (C_{3+} alcohols; +21%), and RP (C_{3+} hydroperoxides; +14%). Finally, the correction of an error in the MVKN yield from its precursor peroxy radical + NO reaction, which had previously

caused a net loss of reactive nitrogen from the mechanism, increases the tropospheric burden of MVKN – a species typically underestimated by models (Tsiligiannis et al., 2022) – by 39%.

5   Conclusions

270   We updated the chemical mechanism of the GEOS-Chem atmospheric chemistry model, used by a large research community for a wide range of applications, with rate coefficient and product branching ratio from recent kinetic data evaluations. A total of 63 reactions were changed, including 58 on the basis of the 2020 JPL Data Evaluation and 5 on the basis of recent IUPAC recommendations. We further updated 63 reactions to improve carbon and nitrogen conservation between reactants and products. We then quantified the effects of these updates on the GEOS-Chem simulation with reference to version 14.0.1 of

275   the model.

Among the most notable changes to the tropospheric burdens of organic species are a 17% decrease in propane due to updates to its OH chemistry, with accompanying changes to its oxidation products (e.g. a 3.5% increase to acetone); a 41% increase in PAA due to its decreased reaction rate coefficient with OH, with accompanying decreases in its downstream products of PAN (-3.8%) and acetic acid (-3.4%); and a 22% reduction in HMHP due to a reduction in the $CH_2OO + H_2O$ rate coefficient, along

280   with a corresponding 3.1% increase in formic acid produced via a competing pathway. A reformulation of the rate coefficient for the CO + OH reaction leads to a 2.7% reduction in the tropospheric CO burden. Eleven updates to reactions of reactive nitrogen species result in a 1.7% net decrease in tropospheric NO_x and a 7% net increase in the stratospheric NO_x burden, with smaller changes to other NO_y species. Updates to the rate coefficients of iodine cycling reactions, especially those of IO with ClO, BrO, and NO, cause minor changes to halogen radical distributions, with general small increases in chlorine

285   radical species and decreases in iodine and bromine species. Most secondary effects on trace gases of general wider interest are also minor, including slight reductions in tropospheric burdens of ozone (-0.7%) and increased loadings of formaldehyde (+0.7%) and OH (+0.3%), the latter of which increases the methane loss rate by a corresponding 0.4%. The updated mechanism will more accurately simulate the complex chemical dependencies of key atmospheric species on temperature, pressure, and concentrations of other compounds, and the improved conservation of carbon and nitrogen will facilitate future studies of their

290   overall atmospheric budgets.

Code and data availability. KPP (Lin et al. (2023), available at https://kpp.readthedocs.io/, last accessed 24 April 2023) and GEOS-Chem (https://geoschem.github.io/, last accessed 24 April 2023; DOI: 10.5281/zenodo.7271974) are both available online for public use. GEOS-Chem mechanism inputs and simulation outputs for this work are available online at "Code and files for 'Technical note: Impacts of updated rate constants on tropospheric composition'", https://doi.org/10.7910/DVN/IDYV3E, Harvard Dataverse, V2, last accessed 30 April 2023.

295   *Author contributions.* KHB, MJE, and BHH conceived and planned this research; KHB performed simulations and analysis; all authors contributed to manuscript preparation.

Competing interests. The authors declare no competing interests.

Acknowledgements. KHB and DJJ acknowledge funding from the U.S. Environmental Protection Agency (EPA) Science to Achieve Results (STAR) grant program (R840014). The views and opinions expressed in this article are those of the authors and do not represent the official
300 views of the EPA.

References

Atkinson, R., Baulch, D. L., Cox, R. A., Crowley, J. N., Hampson, R. F., Hynes, R. G., Jenkin, M. E., Rossi, M. J., and Troe, J.: Evaluated kinetic and photochemical data for atmospheric chemistry: Volume II – gas phase reactions of organic species, Atmospheric Chemistry and Physics, 6, 3625–4055, https://doi.org/10.5194/acp-6-3625-2006, 2006.

305   Baasandorj, M., Fleming, E. L., Jackman, C. H., and Burkholder, J. B.: O(1D) kinetic study of key ozone depleting substances and greenhouse gases, J. Phys. Chem. A, 117, 2434–2445, https://doi.org/10.1021/jp312781c, 2013.

Baeza-Romero, M. T., Glowacki, D. R., Blitz, M. A., Heard, D. E., Pilling, M. J., Rickard, A. R., and Seakins, P. W.: A combined experimental and theoretical study of the reaction between methylglyoxal and OH/OD radical: OH regeneration, Phys. Chem. Chem. Phys., 9, 4114–4128, https://doi.org/10.1039/B702916K, 2007.

310   Bates, K. H. and Jacob, D. J.: A new model mechanism for atmospheric oxidation of isoprene: global effects on oxidants, nitrogen oxides, organic products, and secondary organic aerosol, Atmospheric Chemistry and Physics, 19, 9613–9640, https://doi.org/10.5194/acp-19-9613-2019, 2019.

Bates, K. H., Jacob, D. J., Li, K., Ivatt, P. D., Evans, M. J., Yan, Y., and Lin, J.: Development and evaluation of a new compact mechanism for aromatic oxidation in atmospheric models, Atmospheric Chemistry and Physics, 21, 18 351–18 374, https://doi.org/10.5194/acp-21-
315   18351-2021, 2021.

Berasategui, M., Amedro, D., Vereecken, L., Lelieveld, J., and Crowley, J. N.: Reaction between $CH_3C(O)OOH$ (peracetic acid) and OH in the gas phase: a combined experimental and theoretical study of the kinetics and mechanism, Atmospheric Chemistry and Physics, 20, 13 541–13 555, https://doi.org/10.5194/acp-20-13541-2020, 2020.

Bey, I., Jacob, D. J., Yantosca, R. M., Logan, J. A., Field, B. D., Fiore, A. M., Li, Q., Liu, H. Y., Mickley, L. J., and Schultz, M. G.: Global
320   modeling of tropospheric chemistry with assimilated meteorology: Model description and evaluation, J. Geophys. Res. - Atmos., 106, 23 073–23 095, https://doi.org/10.1029/2001JD000807, 2001.

Bian, H. and Prather, M. J.: Fast-J2: Accurate Simulation of Stratospheric Photolysis in Global Chemical Models, Journal of Atmospheric Chemistry, 41, 281–296, https://doi.org/10.1023/A:1014980619462, 2002.

Burkholder, J. B., Mellouki, A., Talukdar, R., and Ravishankara, A. R.: Rate coefficients for the reaction of OH with HONO between 298
325   and 373 K, International Journal of Chemical Kinetics, 24, 711–725, https://doi.org/https://doi.org/10.1002/kin.550240805, 1992.

Burkholder, J. B., Sander, S. P., Abbatt, J., Barker, J. R., Huie, R. E., Kolb, C. E., Kurylo, M. J., Orkin, V. L., Wilmouth, D. M., and Wine, P. H.: Chemical kinetics and photochemical data for use in atmospheric studies, Evaluation No. 18, Tech. Rep. JPL Publication 15-10, Jet Propulsion Laboratory, Pasadena, CA, 2015.

Burkholder, J. B., Sander, S. P., Abbatt, J., Barker, J. R., Cappa, C., Crounse, J. D., Dibble, T. S., Huie, R. E., Kolb, C. E., Kurylo, M. J.,
330   Orkin, V. L., Percival, C. J., Wilmouth, D. M., and Wine, P. H.: Chemical kinetics and photochemical data for use in atmospheric studies, Evaluation No. 19, Tech. Rep. JPL Publication 19-5, Jet Propulsion Laboratory, Pasadena, CA, 2020.

Chen, Q., Schmidt, J. A., Shah, V., Jaeglé, L., Sherwen, T., and Alexander, B.: Sulfate production by reactive bromine: Implications for the global sulfur and reactive bromine budgets, Geophys. Res. Lett., 44, 7069–7078, https://doi.org/10.1002/2017GL073812, 2017.

DeMore, W. B., Golden, D. M., Hampson, R. F., Howard, C. J., Kolb, C. E., Kurylo, M. J., Molina, M. J., Ravishankara, A. R., and Sander,
335   S. P.: Chemical kinetics and photochemical data for use in atmospheric studies, Evaluation No. 12, Tech. Rep. JPL Publication 97-4, Jet Propulsion Laboratory, Pasadena, CA, 1997.

Dulitz, K., Amedro, D., Dillon, T. J., Pozzer, A., and Crowley, J. N.: Temperature-(208-318 K) and pressure-(18-696 Torr) dependent rate coefficients for the reaction between OH and HNO_3, Atmospheric Chemistry and Physics, 18, 2381–2394, https://doi.org/10.5194/acp-18-2381-20, 2018.

340 Eastham, S. D., Weisenstein, D. K., and Barrett, S. R.: Development and evaluation of the unified tropospheric–stratospheric chemistry extension (UCX) for the global chemistry-transport model GEOS-Chem, Atmospheric Environment, 89, 52–63, https://doi.org/10.1016/j.atmosenv.2014.02.001, 2014.

Fisher, J. A., Jacob, D. J., Travis, K. R., Kim, P. S., Marais, E. A., Chan Miller, C., Yu, K., Zhu, L., Yantosca, R. M., Sulprizio, M. P., Mao, J., Wennberg, P. O., Crounse, J. D., Teng, A. P., Nguyen, T. B., St. Clair, J. M., Cohen, R. C., Romer, P., Nault, B. A., Wooldridge, P. J.,

345 Jimenez, J. L., Campuzano-Jost, P., Day, D. A., Hu, W., Shepson, P. B., Xiong, F., Blake, D. R., Goldstein, A. H., Misztal, P. K., Hanisco, T. F., Wolfe, G. M., Ryerson, T. B., Wisthaler, A., and Mikoviny, T.: Organic nitrate chemistry and its implications for nitrogen budgets in an isoprene- and monoterpene-rich atmosphere: constraints from aircraft (SEAC[4]RS) and ground-based (SOAS) observations in the Southeast US, Atmospheric Chemistry and Physics, 16, 5969–5991, https://doi.org/10.5194/acp-16-5969-2016, 2016.

Fritz, T. M., Eastham, S. D., Emmons, L. K., Lin, H., Lundgren, E. W., Goldhaber, S., Barrett, S. R. H., and Jacob, D. J.: Implementation and

350 evaluation of the GEOS-Chem chemistry module version 13.1.2 within the Community Earth System Model v2.1, Geosci. Model Dev., 15, 8669–8704, https://doi.org/10.5194/gmd-15-8669-2022, 2022.

Guenther, A. B., Jiang, X., Heald, C. L., Sakulyanontvittaya, T., Duhl, T., Emmons, L. K., and Wang, X.: The Model of Emissions of Gases and Aerosols from Nature version 2.1 (MEGAN2.1): an extended and updated framework for modeling biogenic emissions, Geoscientific Model Development, 5, 1471–1492, https://doi.org/10.5194/gmd-5-1471-2012, 2012.

355 Hoesly, R. M., Smith, S. J., Feng, L., Klimont, Z., Janssens-Maenhout, G., Pitkanen, T., Seibert, J. J., Vu, L., Andres, R. J., Bolt, R. M., Bond, T. C., Dawidowski, L., Kholod, N., Kurokawa, J.-I., Li, M., Liu, L., Lu, Z., Moura, M. C. P., O'Rourke, P. R., and Zhang, Q.: Historical (1750–2014) anthropogenic emissions of reactive gases and aerosols from the Community Emissions Data System (CEDS), Geoscientific Model Development, 11, 369–408, https://doi.org/10.5194/gmd-11-369-2018, 2018.

Holmes, C. D., Bertram, T. H., Confer, K. L., Graham, K. A., Ronan, A. C., Wirks, C. K., and Shah, V.: The Role of Clouds in the Tropo-

360 spheric NO_x Cycle: A New Modeling Approach for Cloud Chemistry and Its Global Implications, Geophys. Res. Lett., 46, 4980–4990, https://doi.org/doi.org/10.1029/2019GL081990, 2019.

Hu, L., Millet, D. B., Baasandorj, M., Griffis, T. J., Turner, P., Helmig, D., Curtis, A. J., and Hueber, J.: Isoprene emissions and impacts over an ecological transition region in the U.S. Upper Midwest inferred from tall tower measurements, Journal of Geophysical Research: Atmospheres, 120, 3553–3571, https://doi.org/10.1002/2014JD022732, 2015.

365 Hu, L., Keller, C. A., Long, M. S., Sherwen, T., Auer, B., Da Silva, A., Nielsen, J. E., Pawson, S., Thompson, M. A., Trayanov, A. L., Travis, K. R., Grange, S. K., Evans, M. J., and Jacob, D. J.: Global simulation of tropospheric chemistry at 12.5 km resolution: performance and evaluation of the GEOS-Chem chemical module (v10-1) within the NASA GEOS Earth system model (GEOS-5 ESM), Geosci. Model Dev., 11, 4603–4620, https://doi.org/10.5194/gmd-11-4603-2018, 2018.

Jenkin, M. and Cox, R.: Kinetics of the gas-phase reaction of OH with nitrous acid, Chemical Physics Letters, 137, 548–552,

370 https://doi.org/https://doi.org/10.1016/0009-2614(87)80627-9, 1987.

Lin, H., Jacob, D. J., Lundgren, E. W., Sulprizio, M. P., Keller, C. A., Fritz, T. M., Eastham, S. D., Emmons, L. K., Campbell, P. C., Baker, B., Saylor, R. D., and Montuoro, R.: Harmonized Emissions Component (HEMCO) 3.0 as a versatile emissions component for atmospheric models: application in the GEOS-Chem, NASA GEOS, WRF-GC, CESM2, NOAA GEFS-Aerosol, and NOAA UFS models, Geoscientific Model Development, 14, 5487–5506, https://doi.org/10.5194/gmd-14-5487-2021, 2021.

375   Lin, H., Long, M. S., Sander, R., Sandu, A., Yantosca, R. M., Estrada, L. A., Shen, L., and Jacob, D. J.: An Adaptive Auto-Reduction Solver for Speeding Up Integration of Chemical Kinetics in Atmospheric Chemistry Models: Implementation and Evaluation in the Kinetic Pre-Processor (KPP) Version 3.0.0, Journal of Advances in Modeling Earth Systems, 15, e2022MS003 293, https://doi.org/10.1029/2022MS003293, 2023.

      Mao, J., Jacob, D. J., Evans, M. J., Olson, J. R., Ren, X., Brune, W. H., Clair, J. M. S., Crounse, J. D., Spencer, K. M., Beaver, M. R.,
380   Wennberg, P. O., Cubison, M. J., Jimenez, J. L., Fried, A., Weibring, P., Walega, J. G., Hall, S. R., Weinheimer, A. J., Cohen, R. C., Chen, G., Crawford, J. H., McNaughton, C., Clarke, A. D., Jaeglé, L., Fisher, J. A., Yantosca, R. M., Le Sager, P., and Carouge, C.: Chemistry of hydrogen oxide radicals (HO_x) in the Arctic troposphere in spring, Atmospheric Chemistry and Physics, 10, 5823–5838, https://doi.org/10.5194/acp-10-5823-2010, 2010.

      Mao, J., Paulot, F., Jacob, D. J., Cohen, R. C., Crounse, J. D., Wennberg, P. O., Keller, C. A., Hudman, R. C., Barkley, M. P., and Horowitz,
385   L. W.: Ozone and organic nitrates over the eastern United States: Sensitivity to isoprene chemistry, J. Geophys. Res. - Atmos., 118, 11,256–11,268, https://doi.org/10.1002/jgrd.50817, 2013.

      Marais, E. A., Jacob, D. J., Jimenez, J. L., Campuzano-Jost, P., Day, D. A., Hu, W., Krechmer, J., Zhu, L., Kim, P. S., Miller, C. C., Fisher, J. A., Travis, K., Yu, K., Hanisco, T. F., Wolfe, G. M., Arkinson, H. L., Pye, H. O. T., Froyd, K. D., Liao, J., and McNeill, V. F.: Aqueous-phase mechanism for secondary organic aerosol formation from isoprene: application to the southeast United States and co-benefit of SO_2
390   emission controls, Atmospheric Chemistry and Physics, 16, 1603–1618, https://doi.org/10.5194/acp-16-1603-2016, 2016.

      Mellouki, A., Ammann, M., Cox, R. A., Crowley, J. N., Herrmann, H., Jenkin, M. E., McNeill, V. F., Troe, J., and Wallington, T. J.: Evaluated kinetic and photochemical data for atmospheric chemistry: volume VIII – gas-phase reactions of organic species with four, or more, carbon atoms ($\geq C_4$), Atmos. Chem. Phys., 21, 4797–4808, https://doi.org/10.5194/acp-21-4797-2021, 2021.

      Millet, D. B., Baasandorj, M., Farmer, D. K., Thornton, J. A., Baumann, K., Brophy, P., Chaliyakunnel, S., de Gouw, J. A., Graus, M.,
395   Hu, L., Koss, A., Lee, B. H., Lopez-Hilfiker, F. D., Neuman, J. A., Paulot, F., Peischl, J., Pollack, I. B., Ryerson, T. B., Warneke, C., Williams, B. J., and Xu, J.: A large and ubiquitous source of atmospheric formic acid, Atmospheric Chemistry and Physics, 15, 6283–6304, https://doi.org/10.5194/acp-15-6283-2015, 2015.

      Murray, L. T.: Lightning NOx and Impacts on Air Quality, Current Pollution Reports, 2, https://doi.org/10.1007/s40726-016-0031-7, 2016.

      Park, R. J., Jacob, D. J., Field, B. D., Yantosca, R. M., and Chin, M.: Natural and transboundary pollution influences on sulfate-nitrate-
400   ammonium aerosols in the United States: Implications for policy, J. Geophys. Res. - Atmos., 109, https://doi.org/10.1029/2003JD004473, 2004.

      Safieddine, S. A., Heald, C. L., and Henderson, B. H.: The global nonmethane reactive organic carbon budget: A modeling perspective, Geophysical Research Letters, 44, 3897–3906, https://doi.org/10.1002/2017GL072602, 2017.

      Sander, S. P., Finlayson-Pitts, B. J., Friedl, R. R., Golden, D. M., Huie, R. E., Keller-Rudek, H., Kolb, C. E., Kurylo, M. J., Molina, M. J.,
405   Moortgat, G. K., Orkin, V. L., Ravishankara, A. R., and Wine, P. H.: Chemical kinetics and photochemical data for use in atmospheric studies, Evaluation No. 15, Tech. Rep. JPL Publication 06-2, Jet Propulsion Laboratory, Pasadena, CA, 2006.

      Sander, S. P., Abbatt, J., Barker, J. R., Burkholder, J. B., Friedl, R. R., Golden, D. M., Huie, R. E., Kolb, C. E., Kurylo, M. J., Moortgat, G. K., Orkin, V. L., and Wine, P. H.: Chemical kinetics and photochemical data for use in atmospheric studies, Evaluation No. 17, Tech. Rep. JPL Publication 10-6, Jet Propulsion Laboratory, Pasadena, CA, 2011.

410   Shah, V., Jacob, D. J., Moch, J. M., Wang, X., and Zhai, S.: Global modeling of cloud water acidity, precipitation acidity, and acid inputs to ecosystems, Atmos. Chem. Phys., 20, 12 223–12 245, https://doi.org/10.5194/acp-20-12223-2020, 2020.

Sherwen, T., Schmidt, J. A., Evans, M. J., Carpenter, L. J., Grossmann, K., Eastham, S. D., Jacob, D. J., Dix, B., Koenig, T. K., Sinreich, R., Ortega, I., Volkamer, R., Saiz-Lopez, A., Prados-Roman, C., Mahajan, A. S., and Ordonez, C.: Global impacts of tropospheric halogens (Cl, Br, I) on oxidants and composition in GEOS-Chem, Atmos. Chem. Phys., 16, 12 239–12 271, https://doi.org/10.5194/acp-16-12239-2016, 2016.

Tsiligiannis, E., Wu, R., Lee, B. H., Salvador, C. M., Priestley, M., Carlsson, P. T. M., Kang, S., Novelli, A., Vereecken, L., Fuchs, H., Mayhew, A. W., Hamilton, J. F., Edwards, P. M., Fry, J. L., Brownwood, B., Brown, S. S., Wild, R. J., Bannan, T. J., Coe, H., Allan, J., Surratt, J. D., Bacak, A., Artaxo, P., Percival, C., Guo, S., Hu, M., Wang, T., Mentel, T. F., Thornton, J. A., and Hallquist, M.: A Four Carbon Organonitrate as a Significant Product of Secondary Isoprene Chemistry, Geophysical Research Letters, 49, https://doi.org/10.1029/2021GL097366, 2022.

Tyndall, G. S., Staffelbach, T. A., Orlando, J. J., and Calvert, J. G.: Rate coefficients for the reactions of OH radicals with Methylglyoxal and Acetaldehyde, International Journal of Chemical Kinetics, 27, 1009–1020, https://doi.org/10.1002/kin.550271006, 1995.

van der Werf, G. R., Randerson, J. T., Giglio, L., van Leeuwen, T. T., Chen, Y., Rogers, B. M., Mu, M., van Marle, M. J. E., Morton, D. C., Collatz, G. J., Yokelson, R. J., and Kasibhatla, P. S.: Global fire emissions estimates during 1997–2016, Earth System Science Data, 9, 697–720, https://doi.org/10.5194/essd-9-697-2017, 2017.

Wang, X., Jacob, D. J., Downs, W., Zhai, S., Zhu, L., Shah, V., Holmes, C. D., Sherwen, T., Alexander, B., Evans, M. J., Eastham, S. D., Neuman, J. A., Veres, P. R., Koenig, T. K., Volkamer, R., Huey, L. G., Bannan, T. J., Percival, C. J., Lee, B. H., and Thornton, J. A.: Global tropospheric halogen (Cl, Br, I) chemistry and its impact on oxidants, Atmospheric Chemistry and Physics, 21, 13 973–13 996, https://doi.org/10.5194/acp-21-13973-2021, 2021.

Weng, H., Lin, J., Martin, R., Millet, D. B., Jaegle, L., Ridley, D., Keller, C., Li, C., Du, M., and Meng, J.: Global high-resolution emissions of soil NOx, sea salt aerosols, and biogenic volatile organic compounds, Scientific Data, 7, https://doi.org/10.1038/s41597-020-0488-5, 2020.

Winiberg, F. A. F., Percival, C. J., Shannon, R., Khan, A. H., Shallcross, D. E., Liu, Y., and Sander, S. P.: Reactions kinetics of OH + HNO_3 under conditions relevant to the upper troposphere / lower stratosphere., Phys. Chem. Chem. Phys., 20, 24 652, https://doi.org/10.1039/C8CP04193H, 2018.